Dedicated to Marius Tucsnak on the occasion of his 60^{th} anniversary

LONG-TIME BEHAVIOR OF A COUPLED HEAT-WAVE SYSTEM USING A STRUCTURE-PRESERVING FINITE ELEMENT METHOD

GHISLAIN HAINE, DENIS MATIGNON, and FLORIAN MONTEGHETTI

Communicated by Nicolae Cîndea

This work is a numerical investigation of the coupling between the heat and wave equations, recast as an interconnection of open port-Hamiltonian systems (pHs). A structure-preserving discretization suited to open pHs, based on a mixed finite element approximation space that includes boundary inputs and outputs, is shown to yield a semi-discrete power balance analogous to the continuous one. In the frequency domain, the semi-discretization captures the finite accumulation point in the spectrum, associated with highly-oscillatory eigenfunctions localized at the interconnection interface. In the time domain, the polynomial and logarithmic energy decays proved by Zhang and Zuazua (Arch. Rational Mech. Anal. 184, 2007) are recovered using a Crank-Nicolson scheme.

AMS 2010 Subject Classification: 65M60, 65L07.

Key words: polynomial decay, logarithmic decay, Port-Hamiltonian systems, structure-preserving method.

1. INTRODUCTION AND MAIN RESULTS

This work, which extends [20], is a numerical study of the stabilization of the 2D wave equation by a heat domain as studied theoretically in [38]. The coupled system is recast as an interconnection of open port-Hamiltonian systems (pHs) and a structure-preserving finite element method is employed.

1.1. Structure and applications of pHs

pHs are dynamical systems with collocated boundary inputs and outputs, endowed with a Hamiltonian functional that satisfies a power balance. The underlying geometric structure is known as a Dirac (resp. Stokes-Dirac) structure in the finite-dimensional (resp. infinite-dimensional) case.

A strength of the port-Hamiltonian approach is its natural handling of boundary interconnections that preserve the pHs structure [16]. As a result the

port-Hamiltonian formalism has proven to be a powerful tool for the modelling and control of complex multi-physics systems. In many cases, spatio-temporal dynamics must be considered and infinite-dimensional port-Hamiltonian models are needed [28, 37]. Standard academic examples such as the transmission line, the shallow water, the beam equations and the reactive Navier-Stokes equations have been investigated in the port-Hamiltonian framework [17, 4].

1.2. **Structure-preserving discretization of pHs**

In order to design control laws it is useful to employ a finite-dimensional approximation that preserves the port-Hamiltonian structure of the original system. It may serve as a design guide such as in control by interconnection. Besides, the preservation of the Dirac structure implies the preservation of the power balance (hence of passivity) as well as other dynamical properties such as stability.

Using mixed finite element approximation spaces and following the idea of *primal–dual* or *dual–primal* weak formulations for *closed* hyperbolic systems [24] to perform structure-preserving spatial discretization, the Partitioned Finite Element Method (PFEM) [15] transforms the Stokes-Dirac structure of the continuous *open* system into a Dirac structure at the semi-discrete level. The structure-preserving nature of the approximation implies that the semi-discrete Hamiltonian (defined as the continuous Hamiltonian evaluated on the approximated solution) satisfies a semi-discrete power balance that mimics the continuous one. This semi-discretization methodology can be applied to a large class of structured evolution systems, not necessarily hyperbolic (see e.g. [31]), and handles boundary controls and observations.

The pHs formalism seems suited to computer codes since each subsystem can be independently discretized before interconnection. As long as the spatial discretization is structure-preserving, the coupled semi-discrete model is also a pHs. One drawback is that this methodology typically results in index-2 differential-algebraic equation (DAE) [8, 35] with both boundary Lagrange multipliers and boundary algebraic equations. This makes consistent initialization of high-order time-integration schemes a challenge.

1.3. **Contributions and outline**

It is proven in [38] that the nature of the energy decay of the coupled heat-wave system is driven by whether the Geometrical Control Condition (GCC) [6] holds. Although the control and stabilization of the wave equation

in isolation is well-understood, especially in the framework of finite-differences discretization [39], this is not the case for the coupled heat-wave system. In particular, the stabilization of the wave equation by a heat domain has not been explored numerically, to the best of the authors' knowledge.

This work is a numerical investigation, using a structure-preserving finite element method, of the heat-wave system studied theoretically in [38]. In the frequency domain, the employed semi-discretization is shown to capture the finite accumulation point in the spectrum, associated with highly-oscillatory eigenfunctions localized at the interconnection interface. In the time domain, the polynomial and logarithmic energy decays proved in [38] are recovered using a Crank-Nicolson scheme. This work extends [20] by: giving a time-harmonic validation case; investigating the spectrum of the coupled system; employing an alternative sparse implementation.

This paper is organized as follows. Section 2 summarizes the heat-wave system considered and the stability results from [38]. Section 3 formulates the heat-wave system as a boundary interconnection of two open pHs through a so-called gyrator interconnection. Section 4 covers the structure-preserving discretization. Numerical results in both time and frequency domains are gathered in Section 5.

2. ENERGY DECAY OF A HEAT-WAVE SYSTEM

The purpose of this section is to summarize the stability results proven in [38].

Let $\Omega \subset \mathbb{R}^n$ be a bounded domain with a $\mathcal{C}^2$ boundary $\Gamma := \partial\Omega$. Choose two open subsets of Ω that satisfy:

$$\Omega_1 \subset \Omega,\ \Omega_2 = \Omega \backslash \overline{\Omega_1},$$

and denote the three possible boundaries by:

$$\Gamma_{\text{int}} = \partial\Omega_1 \cap \partial\Omega_2,\ \Gamma_i = \partial\Omega_i \backslash \overline{\Gamma_{\text{int}}},$$

and $\boldsymbol{n}_j$ the unit outward normal vector to Ω_j, see Figure 2.1.

We consider the following coupled partial differential equations (PDEs), $\forall t > 0$:

$$\left\{ \begin{array}{rcll} \partial_t \theta(t,\boldsymbol{x}) - \Delta\theta(t,\boldsymbol{x}) &=& 0, & \boldsymbol{x} \in \Omega_1, \\ \theta(t,\boldsymbol{x}) &=& 0, & \boldsymbol{x} \in \Gamma_1, \\ \partial_{tt} w(t,\boldsymbol{x}) - \Delta w(t,\boldsymbol{x}) &=& 0, & \boldsymbol{x} \in \Omega_2, \\ w(t,\boldsymbol{x}) &=& 0, & \boldsymbol{x} \in \Gamma_2, \end{array} \right. \tag{2.1}$$

together with transmission conditions across the boundary Γ_{int}:

$$\left\{ \begin{array}{rcl} \theta(t,\boldsymbol{x}) &=& \partial_t w(t,\boldsymbol{x}), \\ \partial_{\boldsymbol{n}_1}\theta(t,\boldsymbol{x}) &=& -\partial_{\boldsymbol{n}_2} w(t,\boldsymbol{x}), \end{array} \right. \quad \forall\ t > 0,\ \boldsymbol{x} \in \Gamma_{\text{int}}, \tag{2.2}$$

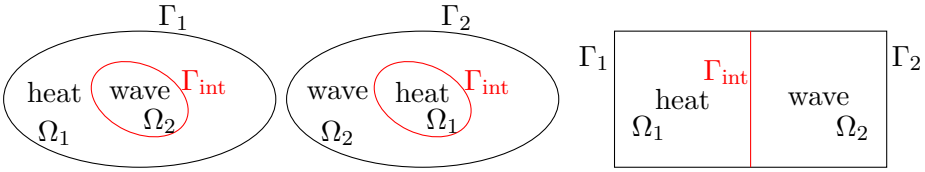

(a) $\Gamma_2 = \varnothing$. (b) $\Gamma_1 = \varnothing$. (c) $\Gamma_1 \neq \varnothing$, $\Gamma_2 \neq \varnothing$.

Fig. 2.1 – Different geometrical configurations

and initial data:

$$\left\{\begin{array}{rcl} \theta(0,\boldsymbol{x}) & = & \theta_0(\boldsymbol{x}), \forall \boldsymbol{x} \in \Omega_1, \\ w(0,\boldsymbol{x}) & = & w_0(\boldsymbol{x}), \forall \boldsymbol{x} \in \Omega_2, \\ \partial_t w(0,\boldsymbol{x}) & = & w_1(\boldsymbol{x}), \forall \boldsymbol{x} \in \Omega_2. \end{array}\right. \tag{2.3}$$

In [38], θ is denoted by y and w by z. However, y is usually used as output of open systems, while z is the state of abstract systems, hence the notation adopted in this work. From [38, Thm. 1], it is known that (2.1)-(2.2) is well-posed in the *finite energy space*:

$$\mathcal{X} := L^2(\Omega_1) \times H^1_{\Gamma_2}(\Omega_2) \times L^2(\Omega_2),$$

endowed with the following norm:

$$\|\boldsymbol{z}\|^2_{\mathcal{X}} := \|z_1\|^2_{L^2(\Omega_1)} + \|z_2\|^2_{L^2(\Omega_2)} + \|\mathbf{grad}\,(z_2)\|^2_{(L^2(\Omega_2))^n} + \|z_3\|^2_{L^2(\Omega_1)}\,. \tag{2.4}$$

Clearly, the semi-norm

$$|\boldsymbol{z}|^2_{\mathcal{X}} := \|z_1\|^2_{L^2(\Omega_1)} + \|\mathbf{grad}\,(z_2)\|^2_{(L^2(\Omega_2))^n} + \|z_3\|^2_{L^2(\Omega_1)}\,,$$

is a norm on $\mathcal{X}$, equivalent to (2.4), when Γ_2 has strictly positive measure. In [38], the asymptotic behaviours of these (semi-)norms have been studied for various geometrical configurations, see Figure 2.1. The theorem below provides a summary of the results of interest from [38].

THEOREM 2.1 (Hamiltonian decay [38]). *Let $n \in \mathbb{N}^*$. Let $\Omega \subset \mathbb{R}^n$ be a bounded domain with smooth boundary. Assume that Γ_{int} is smooth and nonempty.*

- *Assume $\Gamma_2 \neq \emptyset$. Then the heat-wave system is asymptotically stable, i.e. $\mathcal{H}$ tends to zero as $t \to \infty$ [38, Thm. 4]. The decay is neither uniform nor exponential [38, Thm. 6].*

- *Assume both Γ_1 and Γ_2 are nonempty. If Ω_1 satisfies the GCC in Ω, then the following polynomial decay holds [38, Thm. 11]:*

$$\mathcal{H}\,(t) \leq \frac{C}{t^\alpha}\,\mathcal{H}(0), \tag{2.5}$$

with $\alpha = 1/6$.

• *With the alternative interconnection* $\theta = w$ *on* Γ_{int}*, the decay is logarithmic [38, Thm. 13]:*

$$\mathcal{H}(t) \leq \frac{C}{\log^{\alpha}(1+t)}\,\mathcal{H}(0), \tag{2.6}$$

where $\alpha \in (0, 1/16)$.

The most technical assumptions have been simplified and we refer the reader to the original paper for the fully rigorous statements. However, we can make the following comments:

• The stability results extend to the case $\Gamma_2 = \emptyset$; in this case, $\lim_{t\to\infty} \mathcal{H}(t)$ can be a non-null constant, due to the existence of a constant stationary solution. In that case, the estimates (2.5,2.6) apply to $\mathcal{H}(t) - \mathcal{H}(\infty)$.

• The lack of exponential decay is linked to the existence of solutions that are mostly localized in the wave domain and almost completely reflected at the interface Γ_{int}. In [38] these solutions are constructed using a WKB approximation (when the interface is flat) or Gaussian beams (when the interface is curved).

• In the derivation of (2.6), the assumption that the interconnection is given by $\theta = w$ is motivated by technical reasons. This alternative interconnection is not considered in this work.

3. HEAT-WAVE SYSTEM AS INTERCONNECTED PORT-HAMILTONIAN SYSTEM

As recalled in the introduction, infinite-dimensional pHs are related to Stokes-Dirac structures. For example, the power balance satisfied by the Hamiltonian functional is encoded in this structure. These abstract concepts are recalled in Section 3.1, which also discusses the link with boundary control systems. Section 3.2 recasts the coupled heat-wave system (2.1–2.2) as an interconnection of two pHs. Section 3.3 provides the weak formulation that will be used for the finite element discretization of Section 4.

Remark 1. The powerful feature of the port-Hamiltonion formalism being its modularity, this section intends to draw the strategy for a systematic way to state coupled partial differential equations within this framework. It is indeed very useful, e.g. at the implementation level, since it is intrinsically *object-oriented* (*objects* being pHs and interconnections).

3.1. **Infinite-dimensional pHs**

Stokes-Dirac structures are the generalization to infinite dimension of Dirac structures. Although Dirac structures can be defined in several equivalent ways [36], not all these definitions carry over to the infinite-dimensional case. The definition provided below is based on the characterization of Dirac structures given by [36, Proposition 2.1]. We first need the following preliminary definition.

Definition 3.1 (Bond space). Let $\mathcal{E}$ be a pre-Hilbert space and $\mathcal{F} := \mathcal{E}'$ its topological dual. The space $\mathcal{B} := \mathcal{F} \times \mathcal{E}$ endowed with the bilinear form:

$$\left\langle\!\left\langle \begin{pmatrix} f^1 \\ e^1 \end{pmatrix}, \begin{pmatrix} f^2 \\ e^2 \end{pmatrix} \right\rangle\!\right\rangle_{\mathcal{B}} := \langle f^1, e^2 \rangle_{\mathcal{F},\mathcal{E}} + \langle f^2, e^1 \rangle_{\mathcal{F},\mathcal{E}}, \quad \forall \begin{pmatrix} f^1 \\ e^1 \end{pmatrix}, \begin{pmatrix} f^2 \\ e^2 \end{pmatrix} \in \mathcal{B}, \tag{3.1}$$

is called a *bond space*, where $\langle \cdot, \cdot \rangle_{\mathcal{F},\mathcal{E}}$ is the duality bracket with respect to the norm of $\mathcal{E}$.

The space $\mathcal{E}$ is called the *effort space* and $\mathcal{F}$ is called the *flow space*.

Definition 3.2 ((Stokes-)Dirac structure). Let $\mathcal{B}$ be a bond space. A subspace $\mathcal{D} \subset \mathcal{B}$ is called a *(Stokes-)Dirac structure* if and only if $\mathcal{D}^{[\perp]} = \mathcal{D}$, where $\mathcal{D}^{[\perp]}$ is the orthogonal companion of $\mathcal{D}$ in $\mathcal{B}$, defined by:

$$\mathcal{D}^{[\perp]} := \left\{ \begin{pmatrix} f^1 \\ e^1 \end{pmatrix} \in \mathcal{B} \;\middle|\; \left\langle\!\left\langle \begin{pmatrix} f^1 \\ e^1 \end{pmatrix}, \begin{pmatrix} f^2 \\ e^2 \end{pmatrix} \right\rangle\!\right\rangle_{\mathcal{B}} = 0, \; \forall \begin{pmatrix} f^2 \\ e^2 \end{pmatrix} \in \mathcal{D} \right\}. \tag{3.2}$$

Remark 2 (Terminology). The "Stokes" in "Stokes-Dirac" can be justified by the fact that the Stokes divergence theorem is typically used to establish that a function subspace satisfies (3.2), see e.g. [28].

To address boundary-controlled and -observed PDEs, the concept of port-boundary modelling, hence (Stokes-)Dirac structures, has been extended, as in [27]. Coupling PDEs then translates in interconnecting (Stokes-)Dirac structures, studied for instance in [26].

Let us give the definition of infinite-dimensional pHs adopted in this work, already given in [12]. Nevertheless, as the general purpose of this work concerns the structure-preserving semi-discretization of the coupled heat-wave system, the rigorous functional framework will not be addressed in the sequel. Briefly, it is based on known results about boundary control systems [33, Chapter 10]. The *extended structure operator* $\mathcal{J}$ is constructed thanks to the linear (time-independent) systems theory (see e.g. [34] and references therein), using the generating operators of the boundary control systems given by the boundary-controlled and -observed PDE under study. An underlying Stokes-Dirac structure can then be obtained as the graph of this extended structure operator

$\mathcal{J}$ (under suitable assumptions), see e.g. [27, Theorem 3.6]. At the semi-discrete level, it is intended to construct a skew-symmetric extended structure matrix J^h, *i.e.* a Dirac structure thanks to its graph, which approximates the Stokes-Dirac structure.

Definition 3.3 (Infinite-dimensional pHs). Consider Hilbert spaces $\mathcal{X}^1$, $\mathcal{X}^2$, $\mathcal{U}$, and a Hamiltonian $\mathcal{H} := \mathcal{X}^1 \to \mathbb{R}$ defining energy storage. A port-Hamiltonian system on $\mathcal{X}^1$ is given by a (constrained) dynamics:

$$\begin{pmatrix} \dot{\alpha}^1 \\ f^2 \end{pmatrix} = \mathcal{J} \begin{pmatrix} \delta_{\alpha^1}\mathcal{H} \\ e^2 \end{pmatrix}, \qquad \gamma \begin{pmatrix} \delta_{\alpha^1}\mathcal{H} \\ e^2 \end{pmatrix} = u, \tag{3.3}$$

where $\delta_{\alpha^1}\mathcal{H}$ is the variational derivative of $\mathcal{H}$ with respect to α^1 in $\mathcal{X}^1$, $\mathcal{J} \in \mathcal{L}(D(\mathcal{J}), \mathcal{X}^1 \times \mathcal{X}^2)$ (typically a differential operator), and $\gamma \in \mathcal{L}(D(\mathcal{J}),\mathcal{U})$ a (typically boundary) control operator, such that $\mathcal{J}$ is *formally skew-symmetric*:

$$\left(\mathcal{J} \begin{pmatrix} e^1 \\ e^2 \end{pmatrix}, \begin{pmatrix} e^1 \\ e^2 \end{pmatrix} \right)_{\mathcal{X}^1 \times \mathcal{X}^2} = 0, \quad \forall \ \begin{pmatrix} e^1 \\ e^2 \end{pmatrix} \in \ker \gamma.$$

The variable α^1 is known as the *energy* variable, while $e^1 := \delta_{\alpha^1}\mathcal{H}$ is known as the *co-energy* variable.

With this definition at hand, provided some technical assumptions (not discussed here) are satisfied, one formally gets the following result:

Proposition 3.1 (Power balance). *The Hamiltonian of an infinite-dimensional port-Hamiltonian system satisfies the following* power balance *along the trajectories:*

$$\frac{\mathrm{d}}{\mathrm{d}t}\mathcal{H}(\alpha^1(t)) = -\left\langle f^2(t), e^2(t) \right\rangle_{(\mathcal{X}^2)',\mathcal{X}^2} + \left\langle y(t), u(t) \right\rangle_{(\mathcal{U})',\mathcal{U}}, \qquad \forall t \geq 0, \tag{3.4}$$

where $y := C \begin{pmatrix} e^1 \\ e^2 \end{pmatrix}$, *with* $C \in \mathcal{L}(D(\mathcal{J}), (\mathcal{U}'))$ *the operator given by:*

$$\left(\mathcal{J} \begin{pmatrix} e^1 \\ e^2 \end{pmatrix}, \begin{pmatrix} e^1 \\ e^2 \end{pmatrix} \right) = \left\langle C \begin{pmatrix} e^1 \\ e^2 \end{pmatrix}, \gamma \begin{pmatrix} e^1 \\ e^2 \end{pmatrix} \right\rangle_{(\mathcal{U})',\mathcal{U}}, \quad \forall \ \begin{pmatrix} e^1 \\ e^2 \end{pmatrix} \in D(\mathcal{J}).$$

To obtain a complete characterisation of the power balance, a constitutive relation $\mathcal{R}(f^2(t), e^2(t)) = 0$ is added to close the system algebraically, and the term $\left\langle f^2(t), e^2(t) \right\rangle_{(\mathcal{X}^2)',\mathcal{X}^2}$ is then fully determined; moreover when it is positive, the closed dynamical system is dissipative and the open dynamical system is lossy.

In the sequel, the heat equation will be recast as (3.3), with Fourier's law as constitutive relation, while the wave equation will lead to a system without algebraic constraints ($\mathcal{J}$ is defined on the unique Hilbert space $\mathcal{X}^1$). In other

words, this formalism is well-suited for both parabolic and hyperbolic systems, with boundary controls and observations, as already stated in [12].

When dealing with quadratic Hamiltonians (*i.e.* weighted norms in Hilbert spaces), the co-energy variable e^1 is linear w.r.t. α^1, given by a bounded symmetric positive-definite operator $Q = Q^\star > 0$ on $\mathcal{X}^1$ as $e^1 := \delta_{\alpha^1}\mathcal{H} = Q\alpha^1$.

If the constitutive relation is also given by $e^2 = Rf^2$ with $R = R^\star > 0$ a bounded symmetric positive-definite operator on $\mathcal{X}^2$, a linear port-Hamiltonian system defined as in Definition 3.3, with quadratic Hamiltonian, rewrites equivalently, in *energy formulation*:

$$\begin{pmatrix} \dot{\alpha}^1 \\ f^2 \end{pmatrix} = \mathcal{J} \begin{pmatrix} Q\alpha^1 \\ Rf^2 \end{pmatrix}, \qquad \gamma \begin{pmatrix} Q^{-1}\alpha^1 \\ R^{-1}f^2 \end{pmatrix} = u,$$

or in *co-energy formulation*:

$$\begin{pmatrix} Q^{-1}\dot{e}^1 \\ R^{-1}e^2 \end{pmatrix} = \mathcal{J} \begin{pmatrix} e^1 \\ e^2 \end{pmatrix}, \qquad \gamma \begin{pmatrix} e^1 \\ e^2 \end{pmatrix} = u. \tag{3.5}$$

The former will induce matrix inversions, which are best avoided numerically. By contrast, the latter lends itself to the finite element method [12]: taking into account the physical parameters only consists in weighting the inner products of $\mathcal{X}^1$ and $\mathcal{X}^2$, and leads to weighted mass matrices, which average the inverse of the physical parameters in space.

3.2. **Boundary control subsystems and coupling**

Each subsystem is written as a boundary control system (see e.g. [33, Chapter 10]) together with collocated observation that fits the pHs framework: *i.e.* with a *formally* skew-symmetric operator.

3.2.a. **Heat equation**

The chosen representation corresponds to the *Lyapunov* case already presented e.g. in [30], with Hamiltonian:

$$\mathcal{H}_1(t) = \frac{1}{2}\int_{\Omega_1} \rho_\theta(\boldsymbol{x})\, \theta^2(t,\boldsymbol{x})\ \mathrm{d}\boldsymbol{x},$$

where ρ_θ denotes the mass density. Denoting $\boldsymbol{J}_Q$ the heat flux and using Fourier's law $\boldsymbol{J}_Q = -\overline{\overline{\boldsymbol{\kappa}}} \cdot \mathbf{grad}\theta$, with $\overline{\overline{\boldsymbol{\kappa}}}$ the thermal conductivity, a bounded symmetric positive-definite tensor, the port-Hamiltonian system in co-energy formulation (temperature and heat flux) reads:

$$\begin{pmatrix} \rho_\theta\, \partial_t\theta \\ \overline{\overline{\boldsymbol{\kappa}}}^{-1} \cdot \boldsymbol{J}_Q \end{pmatrix} = \begin{bmatrix} 0 & -\mathrm{div} \\ -\mathbf{grad} & 0 \end{bmatrix} \begin{pmatrix} \theta \\ \boldsymbol{J}_Q \end{pmatrix}. \tag{3.6}$$

Added to this system are the collocated boundary controls and observations, *i.e.* the boundary ports:

$$\left\{\begin{array}{rcl} \boldsymbol{J}_Q(t,\boldsymbol{x})\cdot\boldsymbol{n}_1(\boldsymbol{x}) &=& -u_1(t,\boldsymbol{x}),\\ y_1(t,\boldsymbol{x}) &=& \theta(t,\boldsymbol{x}),\end{array}\right. \qquad \forall\, t>0,\, \boldsymbol{x}\in\Gamma_{\rm int}, \tag{3.7}$$

$$\left\{\begin{array}{rcl} \theta(t,\boldsymbol{x}) &=& u_\theta(t,\boldsymbol{x})=0,\\ -y_\theta(t,\boldsymbol{x}) &=& \boldsymbol{J}_Q(t,\boldsymbol{x})\cdot\boldsymbol{n}_1(\boldsymbol{x}),\end{array}\right. \qquad \forall\, t>0,\, \boldsymbol{x}\in\Gamma_1. \tag{3.8}$$

The following result is well-known:

LEMMA 3.2. *The power balance of the open heat subsystem reads:*

$$\frac{\mathrm{d}}{\mathrm{d}t}\mathcal{H}_1 = -\left\|\mathbf{grad}\theta\right\|^2_{L^2_{\overline{\overline{\boldsymbol{\kappa}}}}(\Omega_1)} + \langle u_1, y_1\rangle_{\Gamma_{\rm int}}\,, \tag{3.9}$$

where $\|\mathbf{grad}\theta\|^2_{L^2_{\overline{\overline{\boldsymbol{\kappa}}}}(\Omega_1)} := \int_{\Omega_1}\mathbf{grad}\theta(t,\boldsymbol{x})\cdot\overline{\overline{\boldsymbol{\kappa}}}(\boldsymbol{x})\cdot\mathbf{grad}\theta(t,\boldsymbol{x})\,\mathrm{d}\boldsymbol{x}$*, and* $\langle\cdot,\cdot\rangle_{\Gamma_{\rm int}}$ *denotes the duality bracket between* $H^{-\frac{1}{2}}(\Gamma_{\rm int})$ *and* $H^{\frac{1}{2}}(\Gamma_{\rm int})$*. The open dynamical subsystem is lossy, since* $\frac{\mathrm{d}}{\mathrm{d}t}\mathcal{H}_1 \le \langle u_1, y_1\rangle_{\Gamma_{\rm int}}$*, (the corresponding closed dynamical subsystem would be dissipative).*

3.2.b. **Wave equation**

The wave equation has been widely studied as a pHs (see e.g. [25, 32] and references therein). The Hamiltonian is the sum of the kinetic and potential energies:

$$\mathcal{H}_2(t) = \frac{1}{2}\int_{\Omega_2}\rho_w(\boldsymbol{x})\left(\partial_t w(t,\boldsymbol{x})\right)^2 + \mathbf{grad}w(t,\boldsymbol{x})\cdot\overline{\overline{\boldsymbol{T}}}(\boldsymbol{x})\cdot\mathbf{grad}w(t,\boldsymbol{x})\,\mathrm{d}\boldsymbol{x},$$

where ρ_w is the mass density and $\overline{\overline{\boldsymbol{T}}}$ Young's modulus, a bounded symmetric positive-definite tensor. Since w is the deflection, $v := \partial_t w$ is the deflection velocity, $\mathbf{grad}w$ the strain and $\boldsymbol{\sigma} := \overline{\overline{\boldsymbol{T}}}\cdot\mathbf{grad}w$ the stress. The pHs in co-energy formulation (velocity and stress) then reads:

$$\begin{pmatrix}\rho_w\,\partial_t v\\ \overline{\overline{\boldsymbol{T}}}^{-1}\cdot\partial_t\boldsymbol{\sigma}\end{pmatrix} = \begin{bmatrix}0 & \mathrm{div}\\ \mathbf{grad} & 0\end{bmatrix}\begin{pmatrix}v\\ \boldsymbol{\sigma}\end{pmatrix}, \tag{3.10}$$

together with collocated boundary ports:

$$\left\{\begin{array}{rcl} v(t,\boldsymbol{x}) &=& u_2(t,\boldsymbol{x}),\\ y_2(t,\boldsymbol{x}) &=& \boldsymbol{\sigma}(t,\boldsymbol{x})\cdot\boldsymbol{n}_2(\boldsymbol{x}),\end{array}\right. \qquad \forall\, t>0,\, \boldsymbol{x}\in\Gamma_{\rm int}, \tag{3.11}$$

$$\left\{\begin{array}{rcl} v(t,\boldsymbol{x}) &=& u_w(t,\boldsymbol{x})=0,\\ y_w(t,\boldsymbol{x}) &=& \boldsymbol{\sigma}(t,\boldsymbol{x})\cdot\boldsymbol{n}_2(\boldsymbol{x}),\end{array}\right. \qquad \forall\, t>0,\, \boldsymbol{x}\in\Gamma_2. \tag{3.12}$$

LEMMA 3.3. *The power balance of the open wave subsystem is:*

$$\frac{\mathrm{d}}{\mathrm{d}t}\mathcal{H}_2 = \langle y_2, u_2 \rangle_{\Gamma_{\mathrm{int}}} . \tag{3.13}$$

This open dynamical subsystem is lossless (the corresponding closed dynamical subsystem would be conservative).

3.2.c. **Interconnection**

The coupling is obtained by a *gyrator* interconnection of the boundary ports on Γ_{int}, meaning that the input of one system is given by the output of the other one. This interconnection is known to preserve the pHs structure [36], in the sense that the coupled system remains a pHs. More precisely, the boundary controls are taken as:

$$\left\{ \begin{array}{rcll} u_1(t,\boldsymbol{x}) & = & -y_2(t,\boldsymbol{x}), & \\ u_2(t,\boldsymbol{x}) & = & y_1(t,\boldsymbol{x}), & \end{array} \right. \quad \forall\, t>0,\, \boldsymbol{x} \in \Gamma_{\mathrm{int}}. \tag{3.14}$$

As a consequence, one easily gets:

LEMMA 3.4. *The power balance for the global Hamiltonian, $\mathcal{H} := \mathcal{H}_1 + \mathcal{H}_2$ for the closed coupled system reads:*

$$\frac{\mathrm{d}}{\mathrm{d}t}\mathcal{H} = -\left\| \mathbf{grad}\theta \right\|^2_{L^2_{\overline{\overline{\boldsymbol{\kappa}}}}(\Omega_1)} \leq 0. \tag{3.15}$$

The closed coupled system is dissipative.

3.3. **Weak formulation**

We gather below the weak formulations suitable for the structure-preserving discretization of Section 4, implemented in Section 5.

3.3.a. **Heat equation**

Let $\boldsymbol{\psi}^1$, φ^1 be smooth test functions (respectively vector-valued and scalar). The weak form of (3.6) reads, after integration by parts of the second line:

$$\left\{ \begin{array}{rcl} \left(\partial_t\theta, \rho_\theta\, \varphi^1\right)_{L^2(\Omega_1)} & = & -\left(\mathrm{div}(\boldsymbol{J}_Q),\, \varphi^1\right)_{L^2(\Omega_1)}, \\ \left(\boldsymbol{J}_Q,\, \overline{\overline{\boldsymbol{\kappa}}}^{-1} \cdot \boldsymbol{\psi}^1\right)_{L^2(\Omega_1)} & = & \left(\theta,\, \mathrm{div}(\boldsymbol{\psi}^1)\right)_{L^2(\Omega_1)} \\ & & -\left\langle \boldsymbol{\psi}^1 \cdot \boldsymbol{n}_1, u_\theta \right\rangle_{\Gamma_1} - \left\langle \boldsymbol{\psi}^1 \cdot \boldsymbol{n}_1, y_1 \right\rangle_{\Gamma_{\mathrm{int}}} . \end{array} \right. \tag{3.16}$$

It has been shown in [11] that the output y_1 is the Lagrange multiplier of the Dirichlet constraint imposing u_1. In Section 5, a finite element method will be applied. This requires informations about functional spaces for efficiency or ease (e.g. for using conforming finite elements). The above weak form (3.16) proves well-defined in the following functional spaces:

$$\theta \in L^2_{\rho_\theta}(\Omega_1) \cap H^1(\Omega_1), \qquad \varphi^1 \in L^2(\Omega_1),$$

for the temperature, where $L^2_{\rho_\theta}(\Omega_1)$ is the ρ_θ-weighted $L^2(\Omega_1)$ space. Equivalently, this means that $\rho_\theta\,\theta$ has to be in $L^2(\Omega_1) \cap \rho_\theta^{-1} H^1(\Omega_1)$. Indeed, while $L^2_{\rho_\theta}(\Omega_1)$ is clear from the first term of the weak formulation, $H^1(\Omega_1)$ is required for the control u_θ and the observation y_1 to be well-defined (by (3.7) and (3.8)). Similarly one gets for the heat flux:

$$\boldsymbol{J}_Q \in L^2_{\overline{\overline{\boldsymbol{T}}}^{-1}}(\Omega_1) \cap H_{\mathrm{div}}(\Omega_1), \qquad \boldsymbol{\psi}^1 \in H_{\mathrm{div}}(\Omega_1).$$

The control u_1 and the observation y_θ in (3.7)–(3.8) that do not appear in the above weak formulation (3.16) are also written in a weak form: let ξ^1 and ξ^{int} be smooth test functions on Γ_1 and Γ_{int} respectively, one obtains:

$$\text{(3.17)} \qquad \left\{ \begin{array}{rcl} \left\langle \boldsymbol{J}_Q \cdot \boldsymbol{n}_1,\, \xi^{\mathrm{int}} \right\rangle_{\Gamma_{\mathrm{int}}} & = & -\left\langle u_1,\, \xi^{\mathrm{int}} \right\rangle_{\Gamma_{\mathrm{int}}}, \\ \left\langle y_\theta,\, \xi^1 \right\rangle_{\Gamma_1} & = & -\left\langle \boldsymbol{J}_Q \cdot \boldsymbol{n}_1,\, \xi^1 \right\rangle_{\Gamma_1}. \end{array} \right.$$

As a consequence for the regularity of θ and $\boldsymbol{J}_Q$, the appropriate functional spaces to be found for ξ^{int} and ξ^1 are:

$$\xi^{\mathrm{int}} \in H^{\frac{1}{2}}(\Gamma_{\mathrm{int}}), \qquad \xi^1 \in H^{\frac{1}{2}}(\Gamma_1).$$

3.3.b. **Wave equation**

The wave equation, studied in e.g. [32], does not present the difficulty of mixed boundary conditions: the same integration by parts will make appear both controls u_w and u_2 directly. Let $\boldsymbol{\psi}^2$, φ^2 be smooth test functions. The weak form of (3.10) reads, after integration by parts of the second line:

$$\text{(3.18)} \qquad \left\{ \begin{array}{rcl} \left(\partial_t v,\, \rho_w\, \varphi^2\right)_{L^2(\Omega_2)} & = & \left(\mathrm{div}(\boldsymbol{\sigma}),\, \varphi^2\right)_{L^2(\Omega_2)}, \\ \left(\partial_t \boldsymbol{\sigma},\, \overline{\overline{\boldsymbol{T}}}^{-1} \cdot \boldsymbol{\psi}^2\right)_{L^2(\Omega_2)} & = & -\left(v,\, \mathrm{div}(\boldsymbol{\psi}^2)\right)_{L^2(\Omega_2)} \\ & & + \left\langle \boldsymbol{\psi}^2 \cdot \boldsymbol{n}_2, u_w \right\rangle_{\Gamma_2} + \left\langle \boldsymbol{\psi}^2 \cdot \boldsymbol{n}_2, u_2 \right\rangle_{\Gamma_{\mathrm{int}}}. \end{array} \right.$$

One can deduce the functional spaces from this weak formulation, as already given in [25]:

$$v \in L^2_{\rho_w}(\Omega_2) \cap H^1(\Omega_2), \qquad \varphi^2 \in L^2(\Omega_2),$$
$$\boldsymbol{\sigma} \in L^2_{\overline{\overline{\boldsymbol{\kappa}}}^{-1}}(\Omega_2) \cap H_{\mathrm{div}}(\Omega_2), \qquad \boldsymbol{\psi}^2 \in H_{\mathrm{div}}(\Omega_2).$$

For the observations y_2 and y_w in (3.11)–(3.12): let ξ^2 be smooth test functions on Γ_2, one obtains:

$$\left\{\begin{array}{rcl} \langle y_2,\, \xi^{\mathrm{int}}\rangle_{\Gamma_{\mathrm{int}}} & = & \langle \boldsymbol{\sigma}\cdot\boldsymbol{n}_2,\, \xi^{\mathrm{int}}\rangle_{\Gamma_{\mathrm{int}}}\,, \\ \langle y_w,\, \xi^2\rangle_{\Gamma_2} & = & \langle \boldsymbol{\sigma}\cdot\boldsymbol{n}_2,\, \xi^2\rangle_{\Gamma_2}\,, \end{array}\right. \tag{3.19}$$

from which one deduces:

$$\xi^2 \in H^{\frac{1}{2}}(\Gamma_2).$$

Note that the required regularity for ξ^{int} is the same as that found for the heat subsystem.

3.3.c. **Interconnection**

Finally, the weak form of the gyrator interconnection (3.14) reads:

$$\left\{\begin{array}{rcl} \langle u_1,\, \xi^{\mathrm{int}}\rangle_{\Gamma_{\mathrm{int}}} & = & -\langle y_2,\, \xi^{\mathrm{int}}\rangle_{\Gamma_{\mathrm{int}}}\,, \\ \langle \xi^{\mathrm{int}},\, u_2\rangle_{\Gamma_{\mathrm{int}}} & = & \langle \xi^{\mathrm{int}},\, y_1\rangle_{\Gamma_{\mathrm{int}}}\,. \end{array}\right. \tag{3.20}$$

The last line requires $\xi^{\mathrm{int}} \in H^{-\frac{1}{2}}(\Gamma_{\mathrm{int}})$, which is less restrictive than before. In order to use conforming finite elements, it will then be sufficient to consider $H^1(\Gamma_\star)$ for every boundary finite element bases.

4. **SEMI-DISCRETIZATION OF HEAT-WAVE SYSTEM**

This section derives the semi-discrete coupled system, as used in the numerical applications of Section 5. The presentation seeks to highlight the generality of the proposed discretization methodology, while avoiding technical results on Dirac structures. Section 4.1 surveys elementary properties of finite-dimensional pHs and is essentially the finite-dimensional variant of 3.1. Section 4.2 summarizes the core principles of PFEM, the employed structure-preserving discretization method. Section 4.3 gathers the semi-discrete formulation.

The main take-away from this section is that application of the PFEM to the coupled heat-wave system leads to (4.9), which is a finite-dimensional pHs endowed with the semi-discrete power balance (4.10), analogous to the continuous one (3.15).

4.1. **Finite-dimensional pHs**

The standard definition of a finite-dimensional pHs is as follows (contrast with Definition 3.3).

Definition 4.1 (Finite-dimensional pHs [36]). Consider a *state space* $\mathcal{X}^1 \simeq \mathbb{R}^N$, a resistive space $\mathcal{X}^2 \simeq \mathbb{R}^N$, a *control space* $\mathcal{U} \simeq \mathbb{R}^P$, $N, P \in \mathbb{N}$, and $\mathcal{H} := \mathcal{X}^1 \to \mathbb{R}$ a *Hamiltonian* defining energy storage. A *port-Hamiltonian system* on $\mathcal{X}^1$ is defined by a Dirac structure:

$$\mathcal{D} \subset \mathcal{B} := (\mathcal{X}^1 \times \mathcal{X}^2 \times \mathcal{U}) \times (\mathcal{X}^1 \times \mathcal{X}^2 \times \mathcal{U}),$$

and a (constrained) dynamics:

$$\left(\begin{pmatrix} \dot{\alpha}^1(t) \\ f^2(t) \\ -y \end{pmatrix}, \begin{pmatrix} \mathbf{grad}_{\alpha^1} \mathcal{H}(t) \\ e^2(t) \\ u \end{pmatrix} \right) \in \mathcal{C}([0,\infty); \mathcal{D}),$$

together with a *constitutive relation* $\mathcal{R}(f^2, e^2) = 0$.

The definition [36, Definition 2.3] deals with so-called *modulated* Dirac structures, i.e. Dirac structures that have a dependency upon the energy variable α. The present work does not need such generality, as the heat-wave system leads to a *constant* Dirac structure.

Proposition 4.1 (Power balance). *The Hamiltonian of a finite-dimensional pHs satisfies the following* power-balance *along the trajectories:*

$$\frac{\mathrm{d}}{\mathrm{d}t} \mathcal{H}(\alpha^1(t)) = -e^2(t)^\top f^2(t) + u(t)^\top y(t), \qquad \forall t \geq 0. \tag{4.1}$$

In practice, the constitutive relation $\mathcal{R}(f^2(t), e^2(t)) = 0$ fully determines the power-balance (4.1). The following result will prove enough to exhibit the Dirac structure of the semi-discrete coupled system.

Proposition 4.2. *Consider a port-Hamiltonian system and assume that the trajectories are solutions of the following system:*

$$\begin{pmatrix} \dot{\alpha}^1(t) \\ f^2(t) \end{pmatrix} = J \begin{pmatrix} \mathbf{grad}_{\alpha_1} \mathcal{H}(t) \\ e^2(t) \end{pmatrix} + Bu(t), \quad y(t) = B^\top \begin{pmatrix} \mathbf{grad}_{\alpha_1} \mathcal{H}(t) \\ e^2(t) \end{pmatrix}, \tag{4.2}$$

where J is a skew-symmetric matrix and B a control matrix, with appropriate sizes.

Then the Dirac structure is given as the graph of the extended structure matrix*:*

$$\overline{J} := \begin{bmatrix} J & B \\ -B^\top & 0 \end{bmatrix}.$$

Proof. [36, Exercise 2, p 17]. □

4.2. **Basics of PFEM**

The principle of the PFEM [12] is to use a mixed finite element approximation space [9] to discretize a *partitioned* weak formulation, i.e. a weak formulation where: (a) only one line has been integrated by parts; (b) boundary traces have been substituted by either an input u or an output y; (c) for each input u (resp. output y) introduced, the corresponding collocated output y (resp. intput u) is introduced in an additional equation. The obtained semi-discrete system is (informally) a boundary-controlled system, where the boundary inputs and outputs are collocated.

The choice of which line is to be integrated by parts is dictated by the desired boundary control [15]. In the terminology of [24] (which focus on closed hyperbolic systems), the choice is between a *primal–dual* or a *dual–primal* weak formulation. As recalled in the introduction, this methodology can (and has been) applied to a wide range of systems.

The PFEM is structure-preserving in the sense that it is associated with a semi-discrete power balance that mimics the continuous one. The passive interconnection of semi-discrete pHs leads to another semi-discrete pHs, thus ensuring an accurate discretization of the power balance for the coupled system.

The partitioned formulation is easy to implement since: (a) each PDE is implemented only once as a pHs with domain (α, e, f) and boundary (u, y) variables; (b) at common boundaries, the passive interconnection of two pHs is reduced to two additional algebraic equations that have standardized forms (namely *gyrator* or *transformer* [14, § 4.3.1]). The systematic nature of this approach enables to couple any number of systems without dramatically increasing the development burden. This flexibility comes at the cost of introducing additional algebraic equations in the weak formulation.

4.3. **Semi-discrete formulation**

To derive the semi-discrete system, we follow the PFEM, whose principles have been outlined in the previous section. The partitioned weak formulation has already been given in Section 3.3. This section is organized as follows. After introducing the employed standard approximation spaces, we explicit the system matrices for the heat equation, the wave equation, and the interconnection law. Lastly, the semi-discrete formulation and power-balance of the coupled heat-wave system are written out.

4.3.a. **Mixed finite element approximation spaces**

For any $k \in \mathbb{N}$, let us introduce the standard approximation spaces [9]

$$RT_k(\Omega, \mathcal{T}_h) \coloneqq \left\{ \boldsymbol{u_h} \in H(\mathrm{div}, \Omega) \,|\, \forall K \in \mathcal{T}_h(\Omega),\, \boldsymbol{u_h}_{|K} \in RT_k(K) \right\},$$

$$CG_k(\Omega, \mathcal{T}_h) \coloneqq \left\{ u_h \in H^1(\Omega) \,|\, \forall K \in \mathcal{T}_h(\Omega),\, u_{h|K} \in P_k(K) \right\},$$

$$DG_k(\Omega, \mathcal{T}_h) \coloneqq \left\{ u_h \in L^2(\Omega) \,|\, \forall K \in \mathcal{T}_h(\Omega),\, u_{h|K} \in P_k(K) \right\},$$

where $\mathcal{T}_h(\Omega)$ denote a triangulation of Ω, $RT_k(K)$ denotes the Raviart-Thomas element of maximum degree $k+1$ [9, (3.12)], and $P_k(K)$ denote the space of polynomials of degree k.

The domain variables are approximated as

(4.3)
$$(\theta^h, {\boldsymbol{J_Q}}^h, v^h, \boldsymbol{\sigma}^h) \in DG_k(\Omega_1, \mathcal{T}_h) \times RT_k(\Omega_1, \mathcal{T}_h) \times DG_k(\Omega_2, \mathcal{T}_h) \times RT_k(\Omega_2, \mathcal{T}_h),$$

while the collocated boundary inputs and outputs are approximated as

$$(u_1^h, y_1^h) \in CG_{k+1}(\Gamma_{\mathrm{int}}, \mathcal{T}_h),\ (u_2^h, y_2^h) \in CG_{k+1}(\Gamma_{\mathrm{int}}, \mathcal{T}_h), \tag{4.4}$$

for the interconnection boundary and

$$(u_\theta^h, y_\theta^h) \in CG_{k+1}(\Gamma_1, \mathcal{T}_h),\ (u_w^h, y_w^h) \in CG_{k+1}(\Gamma_2, \mathcal{T}_h), \tag{4.5}$$

for the external boundaries.

4.3.b. **Heat equation**

The considered heat equation has mixed Dirichlet–Neumann boundary conditions on $\partial\Omega_1$; as recalled in Section 3.2 it defines a pHs when equipped with the Hamiltonian $\mathcal{H}_1$. Let

$$(\varphi_j^1)_{1\le j\le N_T},\ (\boldsymbol{\psi}_i^1)_{1\le i\le N_Q},\ (\xi_k^1)_{1\le k\le N_{\Gamma_1}},\ (\xi_k^{\mathrm{int}})_{1\le k\le N_{\Gamma_{\mathrm{int}}}},$$

be the standard bases of

$$DG_k(\Omega_1, \mathcal{T}_h),\ RT_k(\Omega_1, \mathcal{T}_h),\ CG_{k+1}(\Gamma_1, \mathcal{T}_h),\ CG_{k+1}(\Gamma_{\mathrm{int}}, \mathcal{T}_h).$$

The finite element approximation of the partitioned weak formulation (3.16–3.17) leads to a DAE of the form:

(4.6)
$$\begin{bmatrix} M_\theta & 0 & 0 & 0 \\ 0 & M_Q & 0 & 0 \\ 0 & 0 & M_1 & 0 \\ 0 & 0 & 0 & M_{\mathrm{int}} \end{bmatrix} \begin{pmatrix} \dot{\underline{\theta}} \\ \dot{\underline{J_Q}} \\ -\dot{\underline{y_\theta}} \\ -\dot{\underline{u_1}} \end{pmatrix} = \begin{bmatrix} 0 & D_1 & 0 & 0 \\ -D_1^\top & 0 & B_1 & B_{\mathrm{int}} \\ 0 & -B_1^\top & 0 & 0 \\ 0 & -B_{\mathrm{int}}^\top & 0 & 0 \end{bmatrix} \begin{pmatrix} \underline{\theta} \\ \underline{J_Q} \\ \underline{u_\theta} \\ \underline{y_1} \end{pmatrix},$$

known as a port-Hamiltonian Differential Algebraic Equation (pHDAE) [8], where $\underline{\star}$ is the column vector that collects the coefficients of the approximation of $\star$ in its respective finite element basis. The matrices are

$$(M_\theta)_{j,i} \coloneqq \left(\varphi_i^1, \rho_\theta\, \varphi_j^1\right)_{L^2(\Omega_1)}, \; (M_Q)_{j,i} \coloneqq \left(\boldsymbol{\psi_i^1}, \overline{\overline{\boldsymbol{\kappa}}}^{-1} \cdot \boldsymbol{\psi_j^1}\right)_{L^2(\Omega_1)},$$

$$(D_1)_{j,i} \coloneqq -\left(\operatorname{div}(\boldsymbol{\psi_i^1}), \varphi_j^1\right)_{L^2(\Omega_1)}, \; (B_\star)_{i,k} \coloneqq -\left(\boldsymbol{\psi_i^1} \cdot \boldsymbol{n_1}, \xi_k^\star\right)_{L^2(\Gamma_\star)}$$

Note that the boundary output $\underline{y_1}$ plays the role of a Lagrange multiplier [11]. Alternative semi-discretizations of the heat equation based on different Hamiltonians are considered in [30].

Let us now summarize the power balance. By introducing the semi-discrete Hamiltonian $\mathcal{H}_1^h$ as the evaluation of $\mathcal{H}_1$ on the approximation $\theta^h := \sum_{j=1}^{N_T} \theta_j \varphi_j^1$, one obtains $\mathcal{H}_1^h = \frac{1}{2}\underline{\theta}^\top M_\theta\, \underline{\theta}$ so that using the structure of (4.6):

$$\frac{\mathrm{d}}{\mathrm{d}t}\mathcal{H}_1^h = -\underline{J_Q}^\top M_Q\, \underline{J_Q} + \underline{u_1}^\top M_{\mathrm{int}}\, \underline{y_1} + \underline{u_\theta}^\top M_1\, \underline{y_\theta}.$$

Under Dirichlet boundary conditions $u_\theta = 0$, the semi-discrete Hamiltonian therefore satisfies a semi-discrete counterpart to (3.9).

4.3.c. **Wave equation**

Similarly, the finite element approximation of the partitioned weak formulation (3.18–3.19) yields the pHDAE:

(4.7)
$$\begin{bmatrix} M_v & 0 & 0 & 0 \\ 0 & M_{\boldsymbol{\sigma}} & 0 & 0 \\ 0 & 0 & M_2 & 0 \\ 0 & 0 & 0 & M_{\mathrm{int}} \end{bmatrix} \begin{pmatrix} \dot{\underline{v}} \\ \dot{\underline{\boldsymbol{\sigma}}} \\ -\underline{y_w} \\ -\underline{y_2} \end{pmatrix} = \begin{bmatrix} 0 & D_2 & 0 & 0 \\ -D_2^\top & 0 & B_2 & B_{\mathrm{int}} \\ 0 & -B_2^\top & 0 & 0 \\ 0 & -B_{\mathrm{int}}^\top & 0 & 0 \end{bmatrix} \begin{pmatrix} \underline{v} \\ \underline{\boldsymbol{\sigma}} \\ \underline{u_w} \\ \underline{u_2} \end{pmatrix}.$$

The semi-discrete Hamiltonian $\mathcal{H}_2^h$ satisfies, when defined as the evaluation of $\mathcal{H}_2$ on the approximated co-energy variables $\boldsymbol{\sigma}^h$ and v^h,

$$\mathcal{H}_2^h = \frac{1}{2}\left(\underline{v}^\top M_v\, \underline{v} + \underline{\boldsymbol{\sigma}}^\top M_{\boldsymbol{\sigma}}\, \underline{\boldsymbol{\sigma}}\right), \; \frac{\mathrm{d}}{\mathrm{d}t}\mathcal{H}_2^h = \underline{u_w}^\top M_2\, \underline{y_w} + \underline{u_2}^\top M_{\mathrm{int}}\, \underline{y_2},$$

which is the semi-discrete counterpart to (3.13) when $u_w = 0$.

4.3.d. **Interconnection**

The projection of (3.20) in the finite element basis $(\xi_k^{\mathrm{int}})_{1 \le k \le N_{\Gamma_{\mathrm{int}}}}$ reads

(4.8)
$$M_{\mathrm{int}}\, \underline{u_1} = -M_{\mathrm{int}}\, \underline{y_2}, \; M_{\mathrm{int}}\, \underline{u_2} = M_{\mathrm{int}}\, \underline{y_1}.$$

4.3.e. **Coupled system**

The whole semi-discrete coupled heat-wave system can be written as

$$\text{Diag}\begin{bmatrix} M_\theta \\ M_Q \\ M_1 \\ M_{\text{int}} \\ M_v \\ M_{\boldsymbol{\sigma}} \\ M_2 \\ M_{\text{int}} \\ M_{\text{int}} \\ M_{\text{int}} \end{bmatrix} \begin{pmatrix} \dot{\underline{\theta}} \\ \underline{J_Q} \\ -\underline{y_\theta} \\ -\underline{u_1} \\ \dot{\underline{v}} \\ \dot{\underline{\boldsymbol{\sigma}}} \\ -\underline{y_w} \\ -\underline{y_2} \\ \underline{u_1} \\ \underline{u_2} \end{pmatrix} = J^h \begin{pmatrix} \underline{\theta} \\ \underline{J_Q} \\ \underline{0} \\ \underline{y_1} \\ \underline{v} \\ \underline{\boldsymbol{\sigma}} \\ \underline{0} \\ \underline{u_2} \\ \underline{y_1} \\ \underline{y_2} \end{pmatrix}, \tag{4.9}$$

where:

$$J^h := \text{Diag}\left(\begin{bmatrix} 0 & D_1 & 0 & 0 \\ -D_1^\top & 0 & B_1 & B_{\text{int}} \\ 0 & -B_1^\top & 0 & 0 \\ 0 & -B_{\text{int}}^\top & 0 & 0 \end{bmatrix}, \begin{bmatrix} 0 & D_2 & 0 & 0 \\ -D_2^\top & 0 & B_2 & B_{\text{int}} \\ 0 & -B_2^\top & 0 & 0 \\ 0 & -B_{\text{int}}^\top & 0 & 0 \end{bmatrix}, \begin{bmatrix} 0 & -M_{\text{int}} \\ M_{\text{int}} & 0 \end{bmatrix} \right).$$

The symmetry (resp. skew-symmetry) of the block diagonal mass matrix (resp. J^h) induces the underlying Dirac structure. The total semi-discrete Hamiltonian $\mathcal{H}^h = \mathcal{H}_1^h + \mathcal{H}_2^h$ then satisfies, using the gyrator interconnection (4.8) and Dirichlet boundary conditions:

$$\frac{\mathrm{d}}{\mathrm{d}t}\mathcal{H}^h = -\underline{J_Q}^\top M_Q \, \underline{J_Q} - \underline{y_2}^\top M_{\text{int}} \, \underline{y_1} + \underline{y_1}^\top M_{\text{int}} \, \underline{y_2} = -\underline{J_Q}^\top M_Q \, \underline{J_Q}, \tag{4.10}$$

which mimics (3.15) with no approximation (compare with [7, 18]). This analogy implies that the employed finite element discretization is structure-preserving for the coupled pHs.

Remark 3 (Interconnection boundary basis). The same finite element basis has been used at the common interface for both the heat and wave systems. Choosing different bases would yield two different mass matrices for the interface on the left hand-side (depending on the subsystem) and a unique rectangular matrix together with its transpose in place of the two instances of M_{int} in J^h.

Remark 4 (Interconnection matrix). The algebraic constraints coming from the gyrator interconnection could be easily reduced by defining an interconnection matrix. However this would involve inverting the boundary mass matrix thus destroying the sparsity of the semi-discrete system.

In Section 5 below, numerical experiments are performed in order to verify whether the semi-discrete system captures the long-time behaviours proved in [38].

5. NUMERICAL RESULTS

This section gathers the numerical results obtained using the coupled formulation from Section 4. Section 5.1 summarizes the implementation, whose validation is covered in Section 5.2. Section 5.3 discusses the computed energy decays by comparing them to the results in [38].

5.1. Implementation

The implementation, carried out in the Python programming language, relies on widely used open-source scientific packages.

The generation of unstructured meshes is done with gmsh [19], where Ω_i and Γ_i are identified through dedicated tags. The finite element approximation spaces are (4.3,4.4,4.5) with $k = 0$. Assembly is done using multiphenics [1], a package that extends fenics [3] by implementing function spaces restricted to a *subset* of the whole computation domain; this is crucial in this work to easily define unknowns on Ω_i and Γ_i only. The obtained finite element matrices are in the PETSc format [13], in which all the sparse matrix computations are done.

Time integration is done using PETSc TS [2] under the implicit form:

$$F(t, z, \dot{z}) = 0 \quad (t > 0)\,,\ z(0) = z_0 \in \mathbb{R}^N, \tag{5.1}$$

with a discrete state:

$$z = \left(\underline{\theta}, \underline{J_Q}, \underline{u_\theta}, \underline{y_\theta}, \underline{u_1}, \underline{y_1}, \underline{v}, \underline{\boldsymbol{\sigma}}, \underline{u_w}, \underline{y_w}, \underline{u_2}, \underline{y_2}\right)$$

of total length N and right-hand side F linear in both z and $\dot{z}$. The number of mesh triangles is denoted N_t. Note that $\nabla_{\dot{z}} F$ is not invertible due to the presence of algebraic equations. During the implicit time integration, the linear systems are solved using the sparse direct solver MUMPS [5], which delivers satisfactory performance for the values of N considered here. The main advantage of MUMPS is that it avoids using an iterative solver, which would

require constructing an efficient preconditioner; our experiments have shown that standard preconditioners are not suited to the pHs form considered here. Post-processing is done using matplotlib [23].

5.2. **Validation on the eigenvalue problem**

Since manufacturing a solution for the heat-wave system is not straightforward, we use as validation case the associated eigenvalue problem: find $(\hat{\theta}, \hat{w}, \lambda) \in H^2(\Omega_1)\backslash\{0\} \times H^2(\Omega_2)\backslash\{0\} \times \lambda$ such that

$$\begin{aligned} &\lambda\hat{\theta} = \Delta\hat{\theta} \quad (x \in \Omega_1),\ \hat{\theta} = 0 \quad (x \in \Gamma_1) \\ &\lambda^2\hat{w} = \Delta\hat{w} \quad (x \in \Omega_2),\ \hat{w} = 0 \quad (x \in \Gamma_2) \\ &\hat{\theta} = \lambda\hat{w},\ \partial_n\hat{\theta} = \partial_n\hat{w} \quad (x \in \Gamma_{\text{int}}). \end{aligned} \tag{5.2}$$

We focus on the rectangular domain (see Figure 2.1c)

$$\Omega_1 = (0, x_i) \times (0, L_y),\ \Omega_2 = (x_i, L_x) \times (0, L_y), \tag{5.3}$$

for which the eigenvalues are known analytically.

PROPOSITION 5.1 (Exact eigenvalues). *Let $L_x > 0$, $L_y > 0$ and $x_i \in (0, L_x)$. The eigenvalues of (5.2,5.3) are the solutions of*

$$\phi\left[x_i^2\left(\lambda + \beta_n^2\right)\right] = -\lambda\frac{L_x - x_i}{x_i}\phi\left[(L_x - x_i)^2\left(\lambda^2 + \beta_n^2\right)\right] \quad (n \in \mathbb{Z}^*), \tag{5.4}$$

where $\beta_n \coloneqq \frac{\pi}{L_y}n$ and $\phi(z) \coloneqq \frac{\tanh\sqrt{z}}{\sqrt{z}}$.

Proof. We look for a non-null solution with separated variables:

$$\begin{aligned} \hat{\theta} &= \sin(\alpha_1 x)\sin(\beta y) \\ \hat{w} &= A\sin(\alpha_2(L_x - x))\sin(\beta y). \end{aligned}$$

The Dirichlet conditions on $\{x = 0\}$, $\{x = L_x\}$, and $\{y = 0\}$ are satisfied. The Dirichlet condition at $\{y = L_y\}$ is satisfied provided that $\beta = \frac{\pi}{L_y}n$ for some $n \in \mathbb{Z}^*$. Injecting in (5.2), we obtain that the coupled PDE is satisfied iff

$$\begin{aligned} &\text{(a)}\quad \lambda = -\left(\alpha_1^2 + \beta^2\right) \quad \text{(b)}\quad \lambda^2 = -\left(\alpha_2^2 + \beta^2\right) \\ &\text{(c)}\quad \sin(\alpha_1 x_i) = \lambda A\sin(\alpha_2(L_x - x_i)) \\ &\text{(d)}\quad \alpha_1\cos(\alpha_1 x_i) = -\alpha_2 A\cos(\alpha_2(L_x - x_i)), \end{aligned}$$

which is a system of 4 equations for the 4 unknowns $(A, \alpha_1, \alpha_2, \lambda)$. To derive an equation on λ only, we eliminate A from the third equation

$$\frac{\tan(\alpha_1 x_i)}{\alpha_1} = -\lambda\frac{\tan(\alpha_2(L_x - x_i))}{\alpha_2}. \tag{5.5}$$

From (a,b) we have $\alpha_1 = \pm\sqrt{-[\lambda+\beta^2]}$ and $\alpha_2 = \pm\sqrt{-[\lambda^2+\beta^2]}$. Since (5.5) is even with respect to α_i, we can inject to obtain

$$\frac{\tan\left(\sqrt{-[\lambda+\beta^2]}x_i\right)}{\sqrt{-[\lambda+\beta^2]}} = -\lambda\frac{\tan\left(\sqrt{-[\lambda^2+\beta^2]}(L_x-x_i)\right)}{\sqrt{-[\lambda^2+\beta^2]}},$$

where $\sqrt{\cdot}$ stands for *any* branch of the square root. Using that both x_i and $L_x - x_i$ are positive, we obtain the claimed identity. □

We now analyze (5.4) to compute the accumulation points of the eigenvalues; we first need the following elementary lemma.

LEMMA 5.2. *The map $\phi : \mathbb{C} \to \mathbb{C}$, defined in Proposition 5.1, is a meromorphic function.*

Proof. Viewed as a map $\mathbb{C}\backslash(-\infty, 0] \to \mathbb{C}$, ϕ is meromorphic as quotient of analytic functions [29, Thm. 15.12]. A Taylor expansion shows that $z = 0$ is not a branch point, so that ϕ can be extended analytically to any $x \in (-\infty, 0]$ with $\phi(-x) \coloneqq \frac{\tan\sqrt{x}}{\sqrt{x}}$. □

PROPOSITION 5.3 (Accumulation points). *Let $L_x > 0$, $L_y > 0$ and $x_i \in (0, L_x)$. The eigenvalues of (5.2,5.3) form a countable set whose accumulation points are ∞ and -1.*

Proof. From Lemma 5.2, for each $n \in \mathbb{Z}^*$ the set of solutions of (5.4) is the zero set of a meromorphic function; as such, it is at most countable with infinity as the only accumulation point [29, Def. 10.41]. This implies that if a finite accumulation point exists, it must occur as $|n| \to \infty$.

To characterize the possible finite accumulation point, we carry out an asymptotic expansion. We first rewrite (5.4) as $-\lambda\frac{L_x-x_i}{x_i} = I_1(\beta_n, \lambda) \times I_2(\beta_n, \lambda)$ where I_1 and I_2 are given by

$$I_1(\beta_n,\lambda) = \frac{\sqrt{(L_x-x_i)^2\,(\lambda^2+\beta_n^2)}}{\sqrt{x_i^2\,(\lambda+\beta_n^2)}},\ I_2(\beta_n,\lambda) = \frac{\tanh\sqrt{x_i^2\,(\lambda+\beta_n^2)}}{\tanh\sqrt{(L_x-x_i)^2\,(\lambda^2+\beta_n^2)}}.$$

The first term expands as $I_1(\beta_n, \lambda) = \frac{L_x-x_i}{x_i}\left[1 + \mathcal{O}\left(\beta_n^{-2}\right)\right]$. Since I_2 expands as $I_2(\beta_n, \lambda) = 1 + \mathcal{O}(e^{-\mu\beta_n})$ for some $\mu > 0$, we obtain

$$\lambda \underset{|n|\to\infty}{=} -1 + \mathcal{O}\left(\frac{1}{\beta_n^2}\right),$$

so that the only possible finite accumulation point is $\lambda = -1$. □

Remark 5 (Compactness). The existence of a countable sequence of eigenvalues accumulating at -1 indicates that the heat-wave system does not have a compact resolvent. This is proven in [38, Thm. 2] for smooth domains in $\mathbb{R}^n$, $n \geq 2$.

The numerical spectrum is obtained by solving the non-Hermitian sparse generalized eigenvalue problem: find $(z, \lambda) \in \mathbb{C}^N \backslash \{0\} \times \mathbb{C}$ such that

$$\nabla_z F \cdot z = -\lambda \nabla_{\dot{z}} F \cdot z. \tag{5.6}$$

The solution of (5.6) is obtained using the Krylov-Schur solver from SLEPc [22]. Both computed and exact eigenvalues are plotted in Figure 5.1a, which shows a satisfactory agreement. As required for asymptotic stability, all non-null eigenvalues belong to the left open half plane. To conclude this section, we discuss two features of this spectrum.

Firstly, for $|\lambda|$ large enough, eigenvalues can be split in two distinct sequences: the first sequence consists of real negative eigenvalues, associated with eigenfunctions oscillating in Ω_1, while the other one consists of almost purely imaginary eigenvalues, associated with slightly-damped eigenfunctions oscillating in Ω_2. The larger $|\lambda|$, the closer these eigenvalues get to those of the uncoupled system

$$\lambda^h_{k,n} = -\left(\left(\frac{k\pi}{x_i}\right)^2 + \beta_n^2\right),\ \lambda^w_{k,n} = \pm i\left[\left(\frac{k\pi}{L_x - x_i}\right)^2 + \beta_n^2\right]^{1/2} \quad \left((k,n) \in [\mathbb{Z}^*]^2\right). \tag{5.7}$$

The strength of the heat-wave coupling can be qualitatively assessed by comparing the computed eigenvalues to (5.7). The fact that some eigenvalues get infinitely close to $i\mathbb{R}$ (due to the ineffectiveness of the heat equation in damping highly-oscillating wave eigenfunctions) is a manifestation of the fact that uniform exponential decay is not achieved [38, Thm. 6].

Secondly, the sequence of eigenvalues that accumulates at -1 is associated with highly-oscillatory modes localized at the interface Γ_{int}. Although not shown here, these interface eigenvalues always exist and accumulate at -1 regardless of the domain shape considered. The proposed discretization is able to compute them for the rectangular domain, as shown in Figure 5.1b. The accurate computation of these eigenfunctions on curved interfaces Γ_{int} is more challenging, although it is not of concern here since they do not influence whether the Hamiltonian decay is logarithmic or polynomial.

Remark 6 (Semi-discrete kernel). Figure 5.1a shows that (5.6) has the additional eigenvalue $\lambda = 0$, which can be explained as follows. The eigenvalue problem (5.6) is the time-harmonic variant of the semi-discrete pHs formulation (4.9). In this formulation the wave equation is solved through the variables

$(v, \boldsymbol{\sigma}) = (\partial_t w, \overline{\overline{\boldsymbol{T}}} \cdot \mathbf{grad} w)$ so that the Dirichlet boundary condition $w = 0$ on Γ_2 is transformed into $\partial_t w = 0$. This implies that (5.6) does not enforce $\hat{w} = 0$ on Γ_2 but $\lambda \hat{w} = 0$, which is undefined for $\lambda = 0$. Numerically, this leads to a cluster of both null and poorly-converged eigenvalues. This is not a practical concern since the associated eigenfunctions do not influence the time-domain behavior of the discrete system.

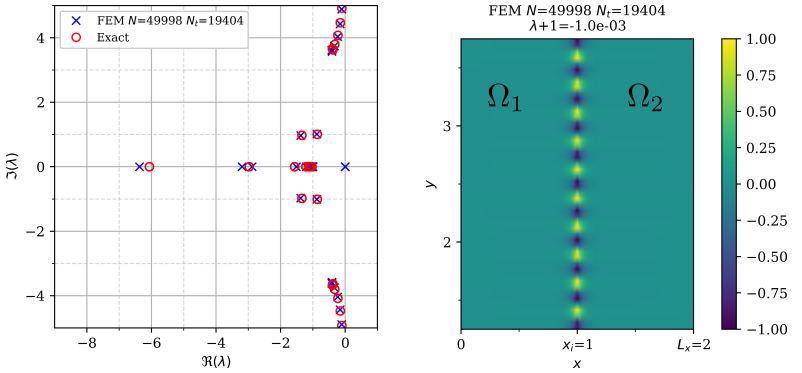

(a) Exact and computed eigenvalues. (b) Eigenfunction (θ^h, v^h) localized at interface.

Fig. 5.1 – Eigenvalues and eigenfunctions on rectangular domain (5.3) with $(L_x, L_y, x_i) = (2, 5, 1)$.

5.3. **Computation of Hamiltonian decay**

This section focuses on the heat-wave system with Dirichlet boundary conditions on Γ_1 and Γ_2, i.e. with boundary inputs u_θ and u_w set to zero. The discretized system is written under the form (5.1), integrated in time with a non-null initial condition z_0, and the computed asymptotic decay rate of the Hamiltonian $\mathcal{H}$ is compared to those stated in Theorem 2.1.

Initial condition

When trying to reproduce the asymptotic behaviors stated in Theorem 2.1 using (5.1), it is useful to keep in mind the following (obvious) remark: since the ODE (5.1) is finite-dimensional, *theoretically* the computed Hamiltonian will decay exponentially as $t \to \infty$. *Practically*, this implies that (5.1) can at best reproduce the theoretical decay rate in some interval $[t_1, t_2]$, where for

$t < t_1$ the asymptotic region has not been entered yet and for $t > t_2$ the decay is exponential. Complicating matters is the use of double precision arithmetic implying that values of $\mathcal{H}^h$ below 10^{-16} cannot be meaningfully considered. Unsuitable choices for z_0 include eigenfunctions (early exponential decay) and constants (boundary conditions not satisfied).

Given the limitations just recalled, in all the time-domain simulations considered below the initial condition z_0 is null except for the wave variable v which is

$$v(t=0) = e^{-\mu|\boldsymbol{x}-\boldsymbol{x_c}|^2}, \tag{5.8}$$

where the parameters μ and $\boldsymbol{x_c}$ are tuned for each domain so that the support lie approximately in the interior of Ω_2. The parameter μ must be small enough for v to be properly resolved on the mesh (otherwise an early exponential damping is observed).

Cases definition

We will focus on the three cases defined below, illustrated in Figure 5.2.

• (Case A) Rectangular domain (5.3) with $(L_x, L_y, x_i) = (2, 1, 1)$. The initial condition is given by (5.8) with $\mu = 20$ and $\boldsymbol{x_c} = (1.5, 0.5)$.

• (Case B) Circular domain with the heat region embedded in the wave region: $\Omega_1 = B(1/2)$ and $\Omega_2 = A\,(1/2, 1)$ where

$$B\,(R) = \{|\boldsymbol{x} - \boldsymbol{x_c}| < R\},\ A\,(R_0, R_1) = \{R_0 < |\boldsymbol{x} - \boldsymbol{x_c}| < R_1\}.$$

Initial condition given by (5.8) with $\mu = 25$ and $\boldsymbol{x_c} = (0.75, 0)$.

• (Case C) Circular domain with the wave region embedded in the heat region: $\Omega_2 = B(1/2)$ and $\Omega_1 = A\,(1/2, 1)$. Initial condition is (5.8) with $\mu = 20$ and $\boldsymbol{x_c} = (0, 0)$.

For all the cases, physical parameters are set to unity.

Time-integration scheme

The main challenge in integrating (5.1) is the computation of a consistent initial state, due to the presence of algebraic variables. We use here a small step of backward Euler (starting from (5.8)) for its ease of implementation, although more sophisticated techniques are available [10]. However, our initialization is usually not accurate enough to enable a stable use of time-adapted high-order schemes, especially for long-time integration (even by taking care of excluding

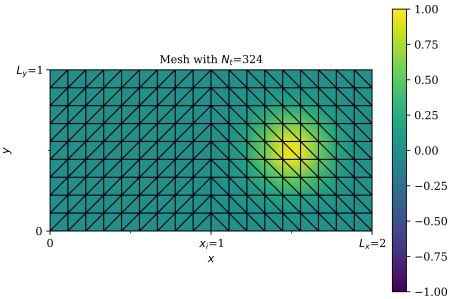

(a) Case A.

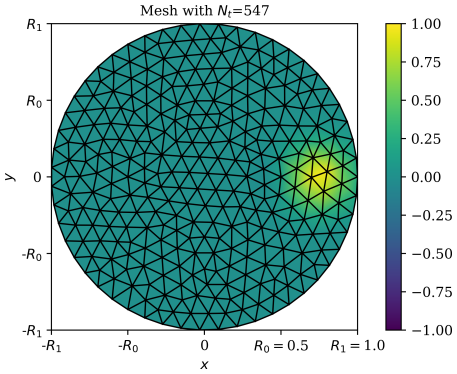

(b) Case B.

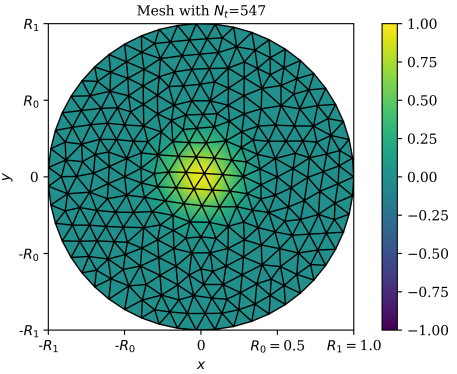

(c) Case C.

Fig. 5.2 – Initial condition on v^h given by (5.8) for a coarse unstructured mesh.

algebraic variables from the local truncation error estimate). We therefore fall back to the second-order Crank-Nicolson scheme with a small time step: this makes for long simulation times (several hours on a laptop) but yields accurate results.

Results

The domains of both cases A and B do not satisfy the GCC. Indeed, in case A the vertical ray $\{x_i = 1.5, y \in (0, L_y)\}$ propagates without reaching Ω_1 while in case B any ray tangential to Γ_{int} propagate in Ω_2 without reaching Ω_1. As a result, Theorem 2.1 suggests that $\mathcal{H}$ must decay logarithmically in both cases, i.e. following (2.6). This contrasts with the domain of case C that does satisfy the GCC, since any ray propagating in Ω_2 does reach Ω_1, so that the polynomial decay (2.5) is expected.

With the initial conditions considered, capturing the asymptotic region in cases A and B require solving until at least $t = 10^6$. Given that we use Crank-Nicolson with a constant time step, the trade-off between simulation

time and accuracy leads us to choosing: in case A, a mesh with $N_t = 324$ ($N = 2000$) and a time step $dt = 0.8$; in case B, $N_t = 2005$ ($N = 5520$) and $dt = 0.85$. Figure 5.3 plots the computed Hamiltonians. The two graphs on the right plot $(H, \log(1+t))$ in logarithmic coordinates, so that the right-hand side of (2.6) is a straight line. Both graphs show a satisfactory agreement.

For illustration, Figure 5.4 plots two eigenfunctions associated with almost purely imaginary eigenvalues. These are functions oscillating in Ω_2 that are poorly damped by the heat region Ω_1: they are therefore close to eigenfunctions of the Dirichlet Laplacian on Ω_2. In case B one can recognize a so-called whispering gallery mode, which propagates energy around the heat region with little loss.

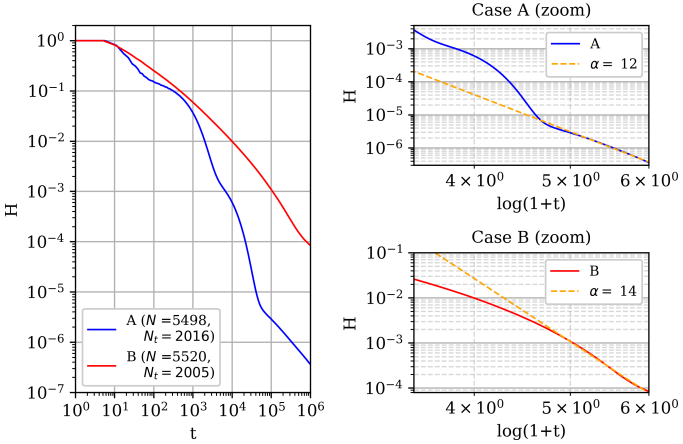

Fig. 5.3 – Hamiltonian decay for cases A and B.

The polynomial decay expected in case C is easier to recover since in our experiments solving until $t = 10^4$ is enough, which enables us to use smaller triangles than in cases A and B. Figure 5.5 plots the Hamiltonian computed for $dt = 0.3$, $N = 119980$, and $N_t = 46985$. The right graph, which plots (H, t) in logarithmic coordinates, shows a satisfactory agreement with the theory.

6. **CONCLUSION**

The above numerical results have shown that the structure-preserving partitioned finite element method is able to quantitatively reproduce the long-time behaviour expected from the theory (see Theorem 2.1). We list below, in no particular order, theoretical and numerical perspectives of this work. The optimality of using CG_k as a boundary approximation space (for collocated outputs and inputs) has been investigated in [21]. Our numerical experiments have

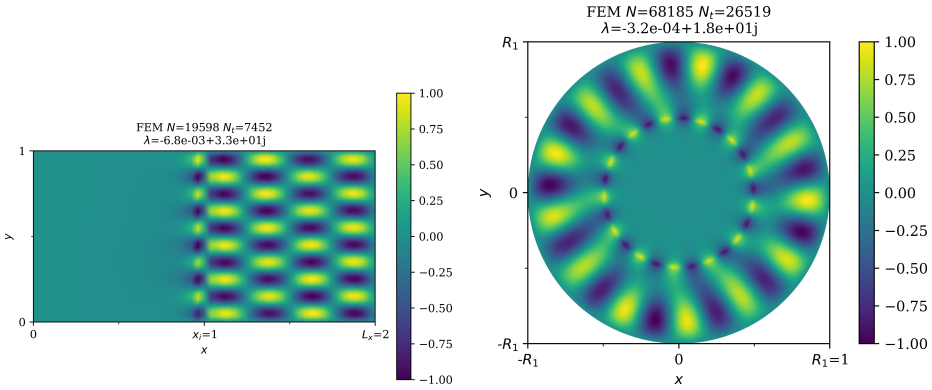

(a) Case A. (b) Case B.

Fig. 5.4 – Poorly-damped eigenfunctions (θ^h, v^h).

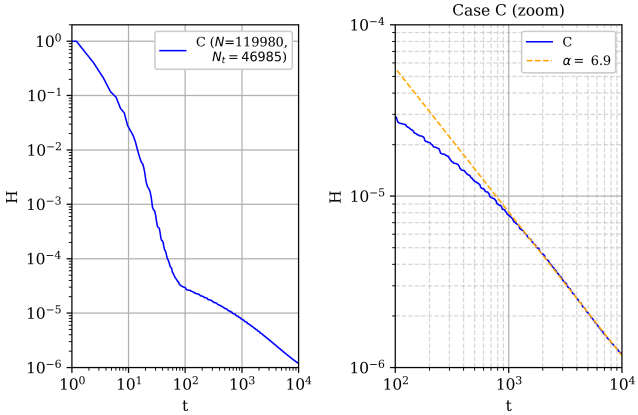

Fig. 5.5 – Hamiltonian decay for case C.

shown that a wrong choice of boundary spaces can lead to unstable eigenvalues, thus rendering the spatial discretization scheme unusable for time-integration purposes. An explanation for this "boundary instability" would be of practical interest. Secondly, although this work has solely focused on the stabilization of the wave equation by a heat domain, additional problems of controllability and observability could be investigated [39].

Thirdly, consistent initialization of the index-2 DAE (5.1) is a challenge, as our experiments have shown that the use of a straightforward backward Euler step can lead to convergence issues with time-adapted schemes. Solutions could include removing algebraic variables as much as possible (after spatial discretization, in a manner transparent to the user) or adapting alternative

initialization techniques designed for index-1 DAEs [10]. Lastly, the use of MUMPS can be considered as a limitation, since it prevents considering extremely large cases (i.e. $N > 10^6$ on a modern laptop for example). The use of an iterative solver would require the design of a preconditionner suited to the proposed pHs formulation.

Acknowledgments. This work has been supported by the AID (Agence de l'Innovation de Défense) from the French Ministry of the Armed Forces (Ministère des Armées).

REFERENCES

[1] Multiphenics. http://mathlab.sissa.it/multiphenics. Accessed: 2010-08-27.

[2] S. Abhyankar, J. Brown, E. M. Constantinescu, D. Ghosh, B. F. Smith, and H Zhang, *PETSc/TS: A Modern Scalable ODE/DAE Solver Library*. ArXiv e-prints, June 2018.

[3] M. Alnæs, J. Blechta, J. Hake, A. Johansson, B. Kehlet, A. Logg, C. Richardson, J. Ring, M. E. Rognes, and G. N. Wells, *The FEniCS Project Version 1.5*. Archive of Numerical Software **3** (2015), *100*.

[4] R. Altmann and P. Schulze, *A port-Hamiltonian formulation of the Navier-Stokes equations for reactive flows*. Systems & Control Letters **100** (2017), 51 – 55.

[5] P. R. Amestoy, A. Buttari, J.-Y. L'Excellent, and T. Mary, *Performance and Scalability of the Block Low-Rank Multifrontal Factorization on Multicore Architectures*. ACM Transactions on Mathematical Software **45** (2019), *1*, Article 2.

[6] C. Bardos, G. Lebeau, and J. Rauch, *Sharp sufficient conditions for the observation, control, and stabilization of waves from the boundary*. SIAM Journal on Control and Optimization **30** (1992), *5*, 1024–1065.

[7] W. Bauer and F. Gay-Balmaz, *Towards a geometric variational discretization of compressible fluids: The rotating shallow water equations*. Journal of Computational Dynamics **6** (2019), *1*, 1–37.

[8] C. Beattie, V. Mehrmann, H. Xu, and H. Zwart. *Linear port-Hamiltonian descriptor systems*. Mathematics of Control, Signals, and Systems **30** (2018), *4*, 1–27.

[9] F. Brezzi and M. Fortin, *Mixed and Hybrid Finite Element Methods*. Springer-Verlag, New York, 1991.

[10] P. N. Brown, A. C. Hindmarsh, and L. R. Petzold, *Consistent Initial Condition Calculation for Differential-Algebraic Systems*. SIAM Journal on Scientific Computing **19** (1998), 1495–1512.

[11] A. Brugnoli, F. L. Cardoso-Ribeiro, G. Haine, and P. Kotyczka, Partitioned Finite Element Method for Power-Preserving Structured Discretization with Mixed Boundary Conditions. IFAC-PapersOnLine **53** (2020), *2*, 7647–7652. 21st IFAC World Congress (invited session).

[12] A. Brugnoli, G. Haine, A. Serhani, and X. Vasseur, *Numerical Approximation of Port-Hamiltonian Systems for Hyperbolic or Parabolic PDEs with Boundary Control*. Journal of Applied Mathematics and Physics **9** (2021), 1278–1321.

[13] E. Bueler, *PETSc for Partial Differential Equations*. SIAM, Philadelphia, 2020.

[14] F. Cardoso-Ribeiro, *Port-Hamiltonian modeling and control of a fluid-structure system - Application to sloshing phenomena in a moving container coupled to a flexible structure.* PhD thesis, Ph. D. Thesis, University of Toulouse, 2016.

[15] F. L. Cardoso-Ribeiro, D. Matignon, and L. Lefèvre, *A partitioned finite element method for power-preserving discretization of open systems of conservation laws.* IMA Journal of Mathematical Control and Information **38** (2021), *2*, 493–533.

[16] J. Cervera, A. J. van der Schaft, and A. Baños, *Interconnection of port-Hamiltonian systems and composition of Dirac structures.* Automatica **43** (2007), *2*, 212–225.

[17] V. Duindam, A. Macchelli, S. Stramigioli, and H. Bruyninckx, *Modeling and Control of Complex Physical Systems: The Port-Hamiltonian Approach.* Springer-Verlag, Berlin Heidelberg, 2009.

[18] H. Egger, *Structure preserving approximation of dissipative evolution problems.* Numerische Mathematik **143** (2019), *1*, 85–106.

[19] C. Geuzaine and J.-F. Remacle, *Gmsh: A 3-D finite element mesh generator with built-in pre- and post-processing facilities.* International Journal for Numerical Methods in Engineering **79** (2009), *11*, 1309–1331.

[20] G. Haine and D. Matignon, *Structure-Preserving Discretization of a Coupled Heat-Wave System, as Interconnected Port-Hamiltonian Systems.* In: F. Nielsen and F. Barbaresco, Eds., *Geometric Science of Information*, Lecture Notes in Computer Science, Vol. 12829, pp. 191–199. Springer, Cham, 2021.

[21] G. Haine, D. Matignon, and A. Serhani, *Numerical analysis of a structure-preserving space-discretization for an anisotropic and heterogeneous boundary controlled N-dimensional wave equation as port-Hamiltonian system.* Preprint arXiv:2006.15032, 2020.

[22] V. Hernandez, J. E. Roman, and V. Vidal, *SLEPc: A scalable and flexible toolkit for the solution of eigenvalue problems.* ACM Transactions on Mathematical Software **31** (2005), *3*, 351–362.

[23] J. D. Hunter, *Matplotlib: A 2D Graphics Environment.* Computing in Science & Engineering **9** (2007), *3*, 90–95.

[24] P. Joly, *Variational Methods for Time-Dependent Wave Propagation Problems.* In: M. Ainsworth, P. Davies, D. Duncan, B. Rynne, and P. Martin, Eds., *Topics in Computational Wave Propagation: Direct and Inverse Problems*, Lecture Notes in Computational Science and Engineering, Vol. 31, pp. 201–264. Springer, Berlin, Heidelberg, 2003.

[25] M. Kurula and H. Zwart, *Linear wave systems on n-D spatial domains.* International Journal of Control **88** (2015), *5*, 1063–1077.

[26] M. Kurula, H. Zwart, A. J. van der Schaft, and J. Behrndt, *Dirac structures and their composition on Hilbert spaces.* Journal of Mathematical Analysis and Applications **372** (2010), *2*, 402–422.

[27] Y. Le Gorrec, H. Zwart, and B. Maschke, *Dirac structures and boundary control systems associated with skew-symmetric differential operators.* SIAM Journal on Control and Optimization **44** (2005), *5*, 1864–1892.

[28] R. Rashad, F. Califano, A. J. van der Schaft, and S. Stramigioli, *Twenty years of distributed port-Hamiltonian systems: a literature review.* IMA Journal of Mathematical Control and Information **37** (2020), 1400–1422.

[29] W. Rudin. *Real and Complex Analysis*. McGraw-Hill Book Company, New York, 3 edition, 1986.

[30] A. Serhani, G. Haine, and D. Matignon. Anisotropic heterogeneous n-D heat equation with boundary control and observation: II. Structure-preserving discretization. *IFAC-PapersOnLine*, 52(7):57–62, 2019. 3rd IFAC Workshop on Thermodynamic Foundations for a Mathematical Systems (TFMST).

[31] A. Serhani, D. Matignon, and G. Haine, *A Partitioned Finite Element Method for the Structure-Preserving Discretization of Damped Infinite-Dimensional Port-Hamiltonian Systems with Boundary Control*. In: F. Nielsen and F. Barbaresco,Eds., *Geometric Science of Information*, Lecture Notes in Computer Science, Vol.11712, pp. 549–558. Springer, Cham, 2019.

[32] A. Serhani, D. Matignon, and G. Haine, *Partitioned Finite Element Method for port-Hamiltonian systems with Boundary Damping: Anisotropic Heterogeneous 2-D wave equations*. IFAC-PapersOnLine **52** (2019), *2*, 96–101. 3rd IFAC Workshop on Control of Systems Governed by Partial Differential Equations (CPDE).

[33] M. Tucsnak and G. Weiss, *Observation and control for operator semigroups*. Birkhäuser Advanced Texts: Basler Lehrbücher. Birkhäuser Verlag, Basel, 2009.

[34] M. Tucsnak and G. Weiss, *Well-posed systems - The LTI case and beyond*. Automatica, 50 (2014), *7*, 1757–1779.

[35] A. J. van der Schaft, *Port-Hamiltonian Differential-Algebraic Systems*. In: *Surveys in differential-algebraic equations. I*, pp. 173–226. Springer Berlin Heidelberg, Berlin, Heidelberg, 2013.

[36] A. J. van der Schaft and D. Jeltsema, *Port-Hamiltonian Systems Theory: An Introductory Overview*. Foundations and Trends® in Systems and Control **1** (2014), *2–3*, 173–378.

[37] A. J. van der Schaft and B. Maschke. *Hamiltonian formulation of distributed-parameter systems with boundary energy flow*. Journal of Geometry and Physics **42** (2002), *1-2*, 166–194.

[38] X. Zhang and E. Zuazua, *Long-time behavior of a coupled heat-wave system arising in fluid-structure interaction*. Arch. Rat. Mech. Anal. **184** (2007), 49–120.

[39] E. Zuazua, *Propagation, observation, and control of waves approximated by finite difference methods*. SIAM Review **47** (2005), *2*, 197–243.

Université de Toulouse
ISAE-SUPAERO
31400 Toulouse, France